Z. Dt. Ges. Geowiss. (J. Appl. Reg. Geol.), **173(4)**, p. 551–564, 14 figs.
Published online January 2023

FloodRisk – Induced seismicity by mine flooding – Observation, characterisation and relation to mine water rise in the eastern Ruhr area (Germany)

Martina Rische, Kasper D. Fischer & Wolfgang Friederich*

Rische, M., Fischer, K. D. & Friederich, W. (2023): FloodRisk – Induced seismicity by mine flooding – Observation, characterisation and relation to mine water rise in the eastern Ruhr area (Germany). – Z. Dt. Ges. Geowiss., 173: 551–564, Stuttgart.

Abstract: As part of the FloodRisk project, the influence of rising mine water in abandoned coal mines on induced seismicity is investigated. The Seismological Observatory of the Ruhr University Bochum operates a monitoring network for the whole Ruhr area (North Rhine-Westphalia, Germany) since 1983. The local scale FloodRisk network was installed in the eastern part of the Ruhr area in 2020. The continuous monitoring opens up the opportunity for a long-term study of seismicity in combination with water levels related to mining in the region. The resulting database for the eastern Ruhr area includes over 13,000 induced earthquakes in a period of 26 years during active mining, very few events in the postmining phase before the onset of flooding and more than 1,700 events in the first two and a half years of flooding. The seismological database is supplemented by the mine water levels, which are regularly measured at various measuring points distributed over the study dewatering area "Haus Aden" and made available by Ruhrkohle Aktiengesellschaft (RAG).

Seismic activity was highest in the phase of active mining and concentrated in the vicinity of the mining areas. After the end of mining, only very low seismicity was detected. With the start of flooding, significantly more events were registered again. The rise curve of the mine water level and the temporal and spatial distribution of the seismicity are observed and analysed. Five temporal flooding phases are identified in which the correlated seismicity shows different distribution patterns. Phases in which the levels of individual sections of the mine merge in flooding show particularly high seismicity. A strong spatial clustering of well-localised events occurs below the deepest flooded levels of the mine. Several mechanisms that alter the stress in active mining and flooded mines and induce seismic events are known from previous studies. To apply this to our study, particular attention is given to the spatial distribution of seismicity in relation to known geologic and mining structures. In the flooding phase, most of the seismicity is localised in the area below the flooded drifts.

Kurzfassung: Im Rahmen des FloodRisk-Projekts wird der Einfluss steigender Grubenwasserpegel in stillgelegten Steinkohlebergwerken auf induzierte Seismizität untersucht. Das Seismologische Observatorium der Ruhr-Universität Bochum betreibt seit 1983 ein Messnetz für das gesamte Ruhrgebiet (Nordrhein-Westfalen, Deutschland). Das lokale FloodRisk-Netzwerk wurde im Jahr 2020 im östlichen Teil des Ruhrgebiets installiert. Die kontinuierliche Überwachung eröffnet die Möglichkeit einer Langzeitstudie der Seismizität in Kombination mit den Pegelständen des Bergbaus in der Region. Die aus der Auswertung der seismologischen Netze resultierende Datenbank umfasst für das östliche Ruhrgebiet über 13.000 induzierte Beben in einem Zeitraum von 26 Jahren während des aktiven Bergbaus, sehr wenige Ereignisse in der Nachbergbauphase vor Beginn der Flutung und mehr als 1.700 Ereignisse in den ersten zweieinhalb Jahren der Flutung. Die seismologische Datenbank wird ergänzt durch die Daten des Grubenwasserspiegels, welche an verschiedenen, über das Untersuchungsgebiet „Haus Aden" verteilten Messpunkten regelmäßig von der Ruhrkohle AG (RAG) gemessen und zur Verfügung gestellt werden. Die seismische Aktivität war während der Phase des aktiven Bergbaus am höchsten und konzentrierte sich auf die Umgebung der Abbaugebiete. Nach dem Ende des Bergbaus wurde nur noch eine sehr geringe Seismizität aufgezeichnet. Mit dem Beginn der Flutung wurden wieder deutlich mehr Ereignisse registriert. Die Anstiegskurve des Grubenwasserspiegels sowie die zeitliche und räumliche Verteilung der Seismizität werden beobachtet und analysiert. Fünf verschiedene Flutungsphasen können identifiziert werden, in denen die korrelierte Seismizität unterschiedliche Verteilungsmuster aufweist. Phasen, in denen sich während des Grubenwasseranstiegs zuvor hydraulisch getrennte Bereiche vereinigen, weisen eine besonders hohe Seismizität auf. Eine starke räumliche Häufung von gut lokalisierten Ereignissen tritt unterhalb der gefluteten tiefsten Sohlen des Bergbaus auf. Aus früheren Studien sind mehrere Mechanismen bekannt, die die Spannung in aktiven Bergwerken und gefluteten Gruben verändern und seismische Ereignisse auslösen. In diesem Zusammenhang wird der räumlichen Verteilung der Seismizität in Bezug auf bekannte geologische und bergbauliche Strukturen besondere Aufmerksamkeit geschenkt. In der Flutungsphase ist der größte Teil der Seismizität auf den Bereich unterhalb der gefluteten Stollen beschränkt.

Keywords: post-mining, induced seismicity, mine water rise, coal mine flooding, Ruhr area

Schlüsselwörter: Nachbergbau, induzierte Seismizität, Grubenwasseranstieg in Steinkohlebergwerken, Ruhrgebiet

*Address of the authors:
Ruhr University Bochum, Faculty of Geosciences, Institute of Geology, Mineralogy and Geophysics, 44780 Bochum, Germany (martina.rische@ruhr-uni-bochum.de)

DOI: 10.1127/zdgg/2023/0346
E. Schweizerbartsche Verlagsbuchhandlung, Stuttgart, Germany, www.schweizerbart.de

1. Introduction

The Ruhr area has been characterised by centuries of mining. Induced stresses from mining-related structures such as shafts, galleries and mining areas overlap with the regional tectonic stress field (Niederhuber et al. 2023, this issue). To enable mining at great depths, the water level in the area of the mines was lowered significantly by intense pumping and the surrounding rock was drained. With the end of coal mining in Germany, concepts have been developed how the so-called eternity tasks can be managed ecologically and economically. Dewatering in the abandoned deep mines plays a major role in this context (RAG 2014). Smaller water provinces are to be merged and the mine water level is to be raised to a higher level to reduce pumping costs. The rising mine water level and the associated increase in pore pressure are now changing the stress conditions again and can lead to induced seismicity.

The FloodRisk project is a multi- and interdisciplinary study of the effects of the rise in mine water level in abandoned coal mine areas in Germany and is reported in a number of studies in this issue: Allgaier et al. 2023; Greve et al. 2023; Niederhuber et al. 2023; Quandt et al. 2023; Ukelis et al. 2023). Effects of mine water rebound include heterogeneous ground uplift, degassing at faults (Ukelis et al. 2023, this issue), and stress changes. One of the most directly measurable effects is the induced seismicity, which is the subject of this paper.

The causes of induced seismicity are diverse (National Research Council 2013; Foulger et al. 2018) and range from fluid extraction or injection (e.g. Zoback & Harjes 1997; Cuenot et al. 2008; Cesca et al. 2011) to artificial water reservoirs (e.g. Talwani 1997; Klose 2012) to surface and deep mining (Seeber et al. 1998; Pechmann et al. 2008; Bischoff et al. 2010; Fritschen 2010), to name a few. Induced events are entirely controlled by anthropogenic stress changes and would have not occurred without them (Dahm et al. 2013).

The stress changes and mechanisms leading to induced seismicity during deep mining in the Ruhr area have been investigated in previous studies (Alber et al. 2009; Bischoff et al. 2010; Wehling-Benatelli et al. 2013). Three models for brittle failure were modelled by Alber et al. (2009) and later identified in a detailed seismological study by Wehling-Benatelli et al. (2013). The first seismic event type occurred near the active advancing face and represents the immediate energy release adjacent to the mined area. The events are spatio-temporally correlated with the migration of the face wall. The second mechanism is associated with the failure of load-bearing sand-/siltstone layers which fail due to enhanced stresses during mining. Induced events cluster slightly above or below the depth of active mining and occurring at the current position of the longwall. The third source mechanism is interpreted as the failure of remnant pillar structures from previously mined out seams overlying the currently excavated seam or tectonically weak structures such as small-scale faults that are reactivated by the mining induced stresses.

It is known from previous studies from different types of mines in Germany (Schütz et al. 2014; Knoll 2016; Alber 2017) that the flooding of old mines can lead to a renewed increase in induced microseismicity. In Schütz et al. (2014), the flooding of a uranium ore deposit (Erzgebirge, Germany), located in the crystalline bedrock, is seismologically monitored. There, weak events are distributed in clusters over the entire deposit area, while stronger events (M_L >0) are linked to local tectonic structures in the granite and shale. Earthquakes occur more frequently in times of high flooding velocities and the deepest quakes also occur during that time. Knoll (2016) considers mechanisms of induced earthquakes in the uranium mine and compares them with those from the first flooding phase in the Saar hard coal mining region (Saarland, southwestern Germany). Events induced by an increased pore fluid pressure dominate in both regions. A study by Alber (2017) analyses 383 events recorded by DMT GmbH & Co. KG during the 2013–2016 mine-water rise in the Duhamel region located also in the Saar hard coal mining region. The mine water rise from below 1,400 m up to 1,072 m is divided into four phases of different rates. The highest seismic activity occurred in the period with the fastest water rise. Epicentres were determined for about half of the observed events and the events were assigned to individual mining areas and a fault zone. By comparing the magnitude and PGV (peak ground velocity) of seismicity during mining and in the flooding period, magnitudes of events on reactivated faults were estimated. The largest induced earthquake in this study was recorded on 9/15/2014 with M_L 2.7 and 7.521 mm/s PGV.

As geological and mining conditions vary greatly between study areas, it is difficult to draw general conclusions about the distribution, frequency and strength of the expected seismicity. More high-resolution studies are also desirable to analyse the induced seismicity during flooding more precisely. Particularly in densely populated areas such as the Ruhr region, it therefore makes sense to conduct investigations accompanying floods in order to be able to prevent damage on the one hand and to conduct basic research on the other.

In this study we focus on the observation of the eastern Ruhr area and investigate in detail the relationship between mine water rise and induced seismicity in the “Haus Aden” dewatering area. The area is tectonically inactive, and all detected earthquakes are induced.

Based on the investigations in the area during active mining (Alber et al. 2009; Bischoff et al. 2010; Wehling-Benatelli et al. 2013) we can estimate which stress changes lead to seismicity in a drained environment. The rise in mine water now adds the influence of increased pore pressure. The distribution of seismicity can provide information if these mechanisms are also activated during flooding. To monitor the induced seismicity during the flooding with high accuracy, we operate a temporal network of up to 29 short period seismic stations since 2020 in the region of the former “Bergwerk Ost” colliery, which had the highest seismicity rate in the Ruhr area during active mining. Continuous monitoring of seismicity and mine water levels is available for this re-

gion from the active mining phase through postmining to the flooding phase.

Section 2 presents the monitoring networks, consisting of permanent seismological stations and an adapted seismological project network, as well as the mine water monitoring stations. Section 3 deals with the setup of the seismological database. For the data of the new network, detection and localisation methods are described. Moreover, this database is analysed from different points of view and correlated with the mine water level data. In section 4 the known geological faults and the mining structures are briefly presented and visualised together with the observed seismicity. In section 5 we discuss how seismic events relate to these structures and how mine water influences the temporal and spatial distribution as well as the failure mechanisms of the events. In addition, the events during flooding are compared in distribution, failure mechanisms and magnitudes with those during mining.

2. Measuring arrangements

2.1 Seismological network

A new temporary local network of seismic stations was installed in 2020 in the eastern Ruhr area to monitor induced seismicity due to changes in the mine water level. The entire region was continuously monitored since 1983 by the seismological observatory of the Ruhr University Bochum (RUB) with the RuhrNet (Ruhr University 2007; Stammler et al. 2021), using different station configurations. Initially seismicity was monitored with a short-period array in the vicinity of the university, later this was extended with local stations in the mining region as well as small time-limited local networks such as HAMNET (Wehling-Benatelli et al. 2013).

The stations of the new FloodRisk network with International Federation of Digital Seismograph Networks (FDSN) network code YD (Friederich et al. 2020) are equipped with short-period sensors and digitisers of different kind (Teledyne Geotech S13 [vertical] + EarthDataLogger, Mark L4-3d + EarthDataLogger, Raspberry shakes 3D/1D). The aperture of the network is about 20 km × 10 km and station spacing ranges between 1 and 3.5 km. In areas with increased seismicity, the station density was increased to improve localisation accuracy. All stations are sending the data online via Seedlink to the RUB seismological observatory, using a Wi-Fi connection or mobile routers. The permanent station RN.HMES (Ruhr University 2007) records data continuously since 2004 and is included in the network. The station configuration changed during the observation period, with the first three stations deployed as early as December 2019, following a 2.6 M_{LV} event. From May to June 2022, the FloodRisk network was expanded to 19 stations and later densified with single stations up to currently 29 short-period seismological stations, shown as triangles in Fig. 1. The temporal change of the network configuration can be seen in Figs. 7–11. The stations are concentrated in the central and eastern parts of the study area, which are particularly active seismically.

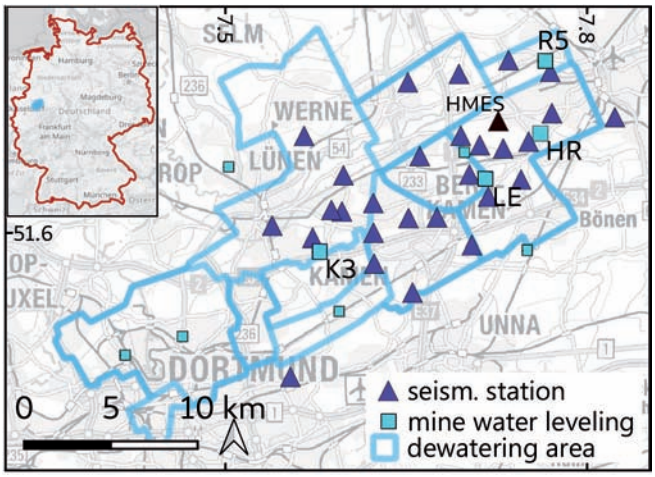

Fig. 1: Map of the water province "Haus Aden", subdivided into subprovinces, in the eastern Ruhr area between the cities of Dortmund and Hamm. The inset at the top left shows the location of the province in Germany. The seismological station network YD, marked by triangles, is concentrated in the central and eastern part of the study area. The seismological station HMES (black triangle) of the RuhrNet is integrated into the FloodRisk monitoring network. Monitoring points of the mine water level measured by RAG are marked by squares. Relevant level changes during the period under investigation can be observed at the shafts Kurl 3 (K3), Lerche (LE), Heinrich Robert (HR) and Radbod 5 (R5).

2.2 Mine water levels

The water rise in the mine workings is monitored with sounding pipes at open shafts. The measuring points are marked as squares in Fig. 1. Levels are measured regularly by RAG and made available via the public web service "Bürgerinformationsdienst" (BID; RAG-BID 2022).

A schematic section through the mine workings (Fig. 2) from the shaft Kurl3 (K3) in SW to the Radbod5 (R5) NE shows the open surface shafts and the deepest levels of the mine. These deepest levels show a strong topography. The black line in the map inlet shows the section between the marked shafts. The section runs through various partial water provinces, which are merged in the flooding process to form one dewatering province as soon as the barriers, such as inclined rock headings, which are also visible in the topography, are exceeded by the water level. The mine water levels in the shafts at different points in time during the project are also shown in this figure. Only the water levels in the shafts, marked as lines in different shades of blue, are known. To what extent the surrounding mountains are already saturated with water is unknown. The porosity of the surrounding rock is very low (Greve et al. 2023) so that flow movements are mainly to be expected in the open mine structures. The main

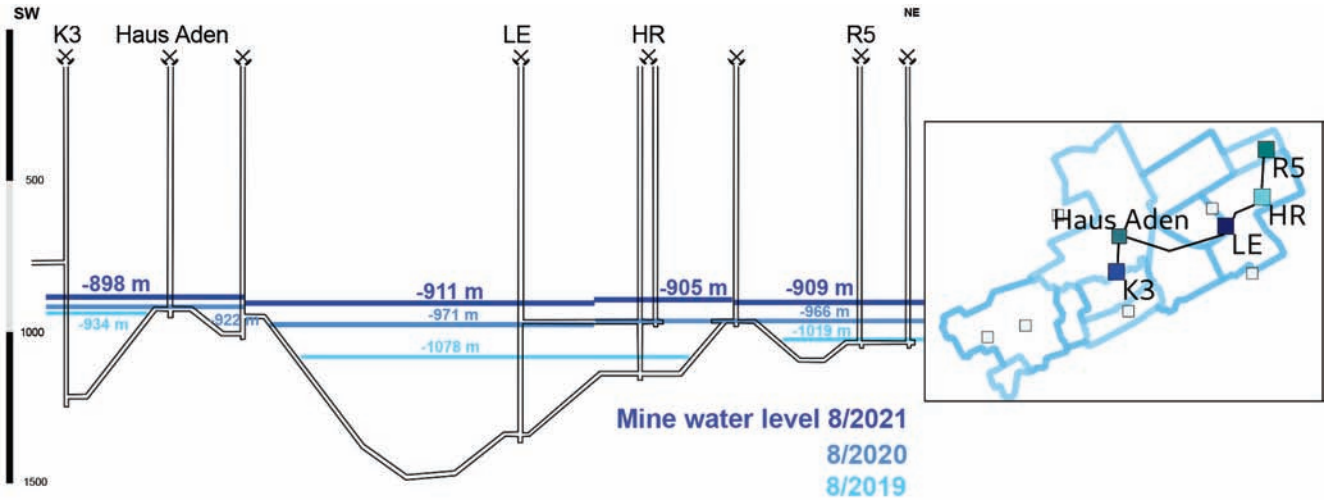

Fig. 2: Schematic section SW to NE through the mine workings of the former "Bergwerk Ost" colliery, showing shafts and deepest levels. The labelled open shafts are equipped with sounding pipes for mine water monitoring. The map shows the location of the section (black line) in the Haus Aden province with the boundaries of the abandoned partial water provinces (blue borders). At the Haus Aden shaft, after reaching the target level, dewatering will be carried out using a submersible pump. Mine water levels at different points in time during the project give an idea of the distribution of mine water underground. The different levels at the beginning of the flooding can be seen, which are initially still separated by inclined rock headings. As the flooding progresses, the levels in the different subareas approach each other. The main hydraulic pathways are the beds, crossways and (opened) pipelines.

waterways are the beds, crosscuts and opened pipelines (Maibaum 2012). After the pumps are shut off, the deep groundwater rises and collects in the open mine structures. The aim of changing of mine water drainage concept is to reduce pumping costs by merging pumping sites into a centralised water drainage system and switching to well operation at a shallower level (-670 m to 600 m in Haus Aden dewatering area; RAG AG 2014). The pumps in the deepest parts of the mine were turned off between 2011 and 2013 after active mining ceased, so some deep levels are already flooded. Unfortunately, this period is not documented by high resolution measurements. After the temporary cessation of pumping in the study area in mid-2019, different levels (light blue lines in Fig. 2) can be seen in individual mine sections, which are separated by inclined rock headings. The water flowing into the mine is diverted to the west in the direction of Haus Aden. Since mid-2020, a uniform water level (medium blue lines in Fig. 2) has been reached in the eastern area and the levels at the shafts Radbod5 (R5), Heinrich Robert (HR) and Lerche (LE) monitoring sites have been rising simultaneously. In mid-2021, the water level at Kurl3 (K3) is also approaching the water level in the eastern area. Unfortunately, water levels for the Haus Aden shaft, where the remaining water is to be pumped after reaching the final level, are only sparsely available (two data points in the observation period) and have not been considered in this study.

3. Observations

3.1 Seismological database

The event database for induced earthquakes during mining and after completion of mining until the construction of the FloodRisk network is based on the annual reports (Harjes 1983–2004; Meier 2005–2006) which contains the localisation of the epicentres and the local magnitudes. Since 2007, the RuhrNet has been registered in the FDSN under the network code RN. The detection threshold changes are depending on the network configuration and evaluation method. Up to May 2019, 13,069 events in the magnitude range between 0 and 3.0 M_L could be evaluated.

In order to obtain a database as complete as possible for induced events during the FloodRisk project, several different approaches are used for detection. The noise level at some stations is quite high due to the urban environment so one automatic detection tool alone either makes too many false predictions or misses smaller events. A denoising method according to Heuel & Friederich (2022) is tested to improve the data quality at some very noisy stations. Events above 0.6 M_{LV} are reliably detected by an automatic system in the processing software SeisComP3 (Helmholtz Centre Potsdam GFZ – German Research Centre for Geosciences & gempa, GmbH 2008) another automatic system uses a similarity analysis to search for events that belong to an already existing cluster and can thus be found based on template events (Gal et al. 2021). In addition, a manual check is done to see whether there are further events not detected by the automatic systems. Particular attention is paid to newly activated focal areas for which no templates are yet available.

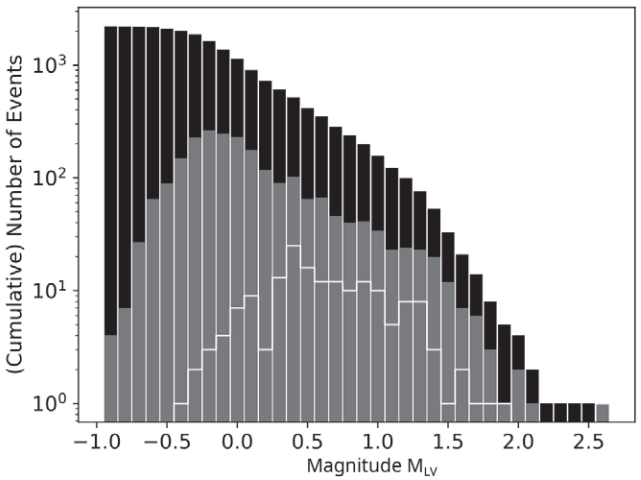

Fig. 3: Cumulative (black) as well as simple (grey) magnitude-frequency distribution in the FloodRisk network for the period from June 2019 to December 2021. The white staircase function shows the magnitude distribution in the still incomplete measurement network until May 2020, which is considered when estimating the completeness of 0.5 M_{LV}.

All detected events are evaluated and verified manually. The processing includes a correction of the automatically determined onsets, a manual adjustment of local P and S phases and a determination of the hypocentre by means of a non-linear localisation in the programme NonLinLoc (Lomax et al. 2000, 2009) from the determined P and S travel times, as well as a magnitude determination. A 1D velocity model is used for localisation. Fritschen et al. (1999) used a model that takes into account the carboniferous strata in the eastern Ruhr area. This model was smoothed and integrated with the regional model of the Ruhr University Observatory.

A total of 1,744 induced events were evaluated in the study area between June 2019 and December 2021 using over 20,000 picked onsets. The magnitudes of the events range between -0.8 and 2.6 M_{LV}, compare Fig. 3 for an overview of the magnitude distribution of the events. For comparative studies, the different detection thresholds depending on the different monitoring networks have to be taken into account. In order to compare the seismicity during the flooding phase with that during active mining and after decommissioning, we assume a completeness of the overall catalogue of 1.4 M_L (Bischoff et al. 2010). For a conservative estimation of the completeness within the FloodRisk network, we have considered, in addition to the total catalogue, the period in which the station network was still extended and thus obtain a value of 0.5 M_{LV} with 365 events above this limit.

3.2 Temporal distribution of seismicity and mine water

The temporal distribution of the induced seismicity in the study area correlates with the mining activities. Fig. 4 shows the temporal pattern of seismicity over the entire database for the Ruhr area from 1983 to 2022. During the active mining phase 50 to 350 induced events with magnitudes above the completeness magnitude of 1.4 M_L (and up to 1,990 events yearly over all magnitudes) were detected in the study area each year. These induced events correlate both temporally and spatially with the extraction activity. Thus, a clear concentration on the working days and hours is evident in the temporal distribution (Bischoff et al. 2010) and, if well localised, the mining progress in the longwall face could be tracked by the localised quakes (Wehling-Benatelli et al. 2013). Seismicity decreased rapidly after mining was stopped and remained at a very low level until the beginning of the flooding phase.

Fig. 5 shows the mine water levels (a), the temporal seismicity distribution (b) and the magnitudes of the events as well as the cumulated energy release (c) from 2000 until end of 2021. Fig. 6 shows the same features in a zoomed-in time window focused on flooding.

With the end of active mining at "Bergwerk Ost" colliery in 2010, the induced seismicity strongly decreases to about 1–2% of the events during active mining. After the shutdown of the pumps mid-2019 in the eastern subarea and the beginning of the mine water rise there, the seismicity increases again. Until 2016, all water levels remain relatively constant. The water level increase at the monitoring station LE from 2016 until 2018 up to the level of the station HR is not reflected in the seismicity. The other stations stay at the same level until the pumps are switched off and partly even beyond. After the pumps are shut down mid-2019, the water level in HR and LE rises only slightly and then sharply from 11/2019. At the same time, the number of measured induced

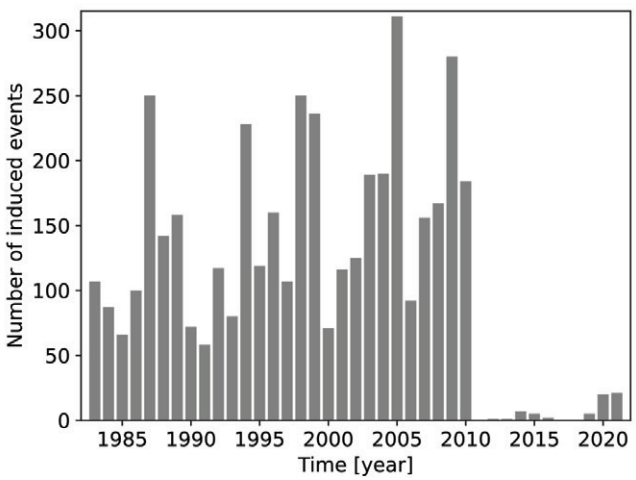

Fig. 4: Display of the total catalogue in the region "Bergwerk Ost", with all evaluated earthquakes from 1983 to 2021 above the completeness threshold of 1.4 M_{LV} as number of events per year. Until 2010, the frequency is between 50 and over 300 events annually. After the end of mining in 2010, only very few earthquakes are recorded, until the activity increases again to about 20 events per year in 2020/2021 with the rebound of mine water in the eastern subprovinces of the Haus Aden dewatering area.

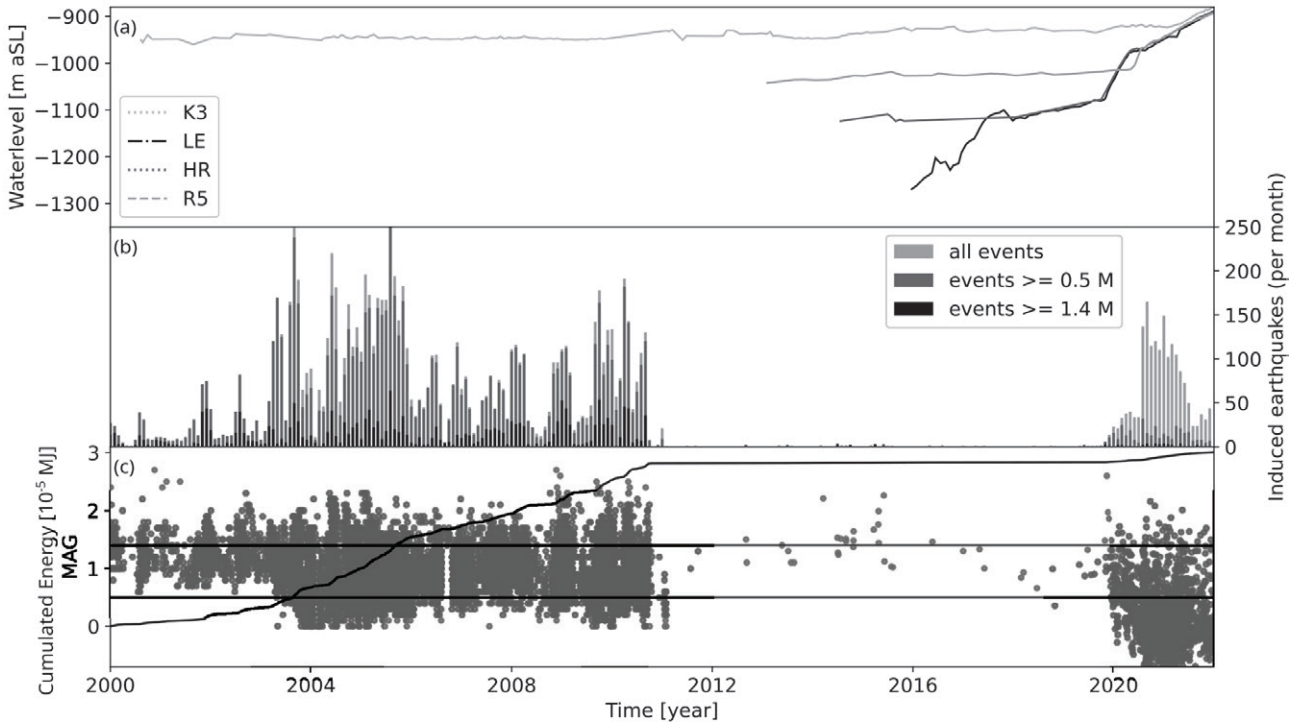

Fig. 5: Temporal variation of mine water levels and measured induced seismicity in the region since 2000. (**a**) Shows the mine water levels at the monitoring stations of RAG HR, K3, LE and R5. (**b**) Shows the monthly number of events, subdivided by the completeness thresholds of the different evaluations, into events from 1.4 M_{LV} in black, above 0.5 M_{LV} (dark grey) and the total number of events in light grey. (**c**) Shows cumulated energy of the seismicity and the temporal sequence of the individual events plotted against their magnitude. The horizontal dashed lines indicate magnitude thresholds 0.5 and 1.4 M_{LV}.

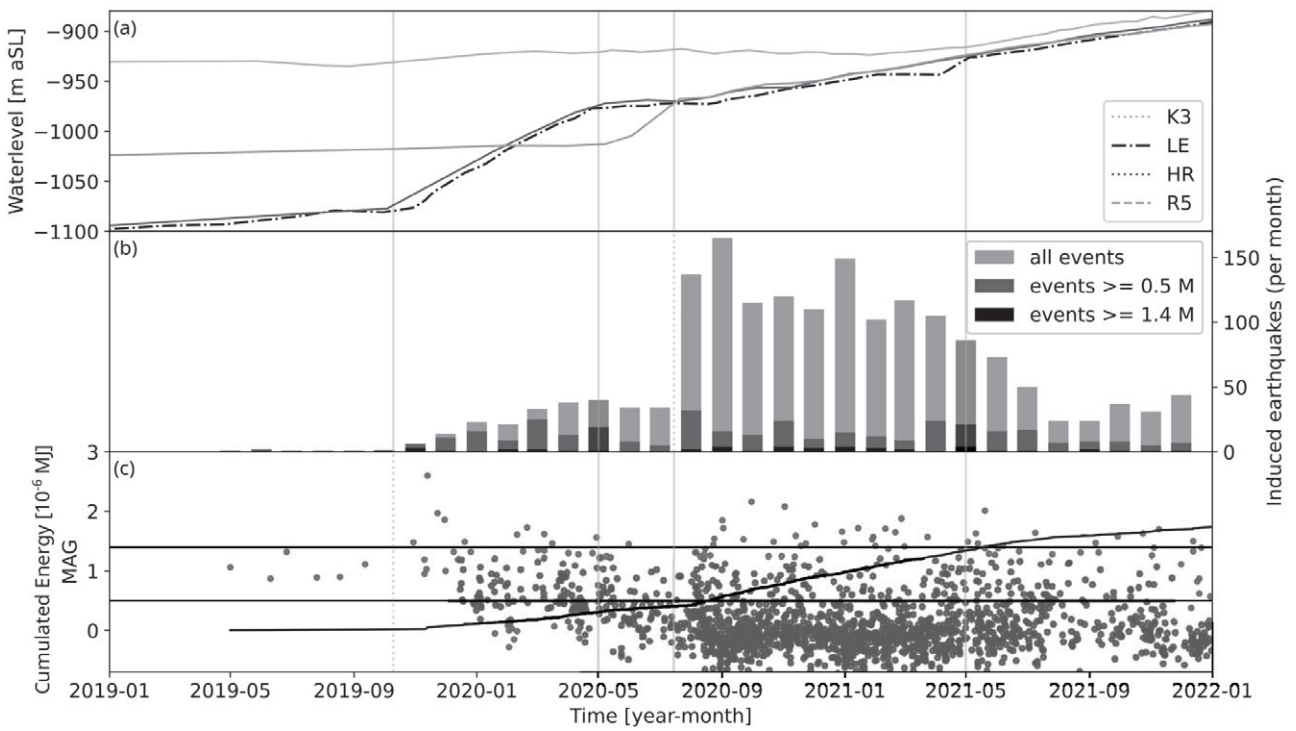

Fig. 6: In order to be able to see details in the temporal variation of the seismicity and the rise of the mine water in the period of the FloodRisk monitoring network, the curves and distributions are shown here since 2019. (**a**) Shows the increase in mine water in the region of the FloodRisk monitoring network, (**b**) indicates the monthly number of seismic events and (**c**) shows the cumulated seismic energy as well as the seismic activity as a function of time and magnitude. Each dot is a single event.

earthquakes (Figs. 6b and c) increases strongly in this area. One of them is the strongest event measured so far in this region after the end of active mining, with a magnitude of 2.6 M_{LV} on 2019-11-13. In April/May, the water levels at HR and LE reach a level of about -975 m and the water rises more slowly. At the same time, the level at R5 starts to rise strongly until it reaches the same level as HR and LE in August (compare Fig. 2) and the levels at the three observation points rise approximately synchronously. The seismic activity, which is mostly localised between the LE, HR and R5 shafts, has increased significantly since the end of 2019. The highest rate is detectable in August/September 2020 and correlates with the parallel increase of the mine water levels at the three surrounding monitoring stations. The mean number of events with a magnitude >0.5 M_{LV} increases to 15 per month. The seismicity is thus significantly higher than during the period between the end of mining and the shutdown of the pumps, but is at most a quarter of the seismicity during the active mining period. The light grey bars of the histogram also include the number of recorded earthquakes with a magnitude below the magnitude of completeness. The increase in seismicity during the flood period would only be approximately visible with the regional stations. With the local FloodRisk network, the detection threshold has been lowered so that detailed studies are possible. In Fig. 5c, the three periods from active mining through the postmining period to flooding are well indicated by the different slopes of the cumulative energy release. In Fig. 6c the slope of the cumulative energy release graph correlates with different phases of flooding, which are discussed in more detail in the next section.

3.3 Spatio-temporal distribution of seismicity

Based on the characteristics of the mine water rise, five temporal phases are defined, for which the spatial distribution of the induced earthquakes is shown in the maps (Figs. 7–11). This allows considering temporal and spatial variations of seismicity in connection with the mine water rise. In the

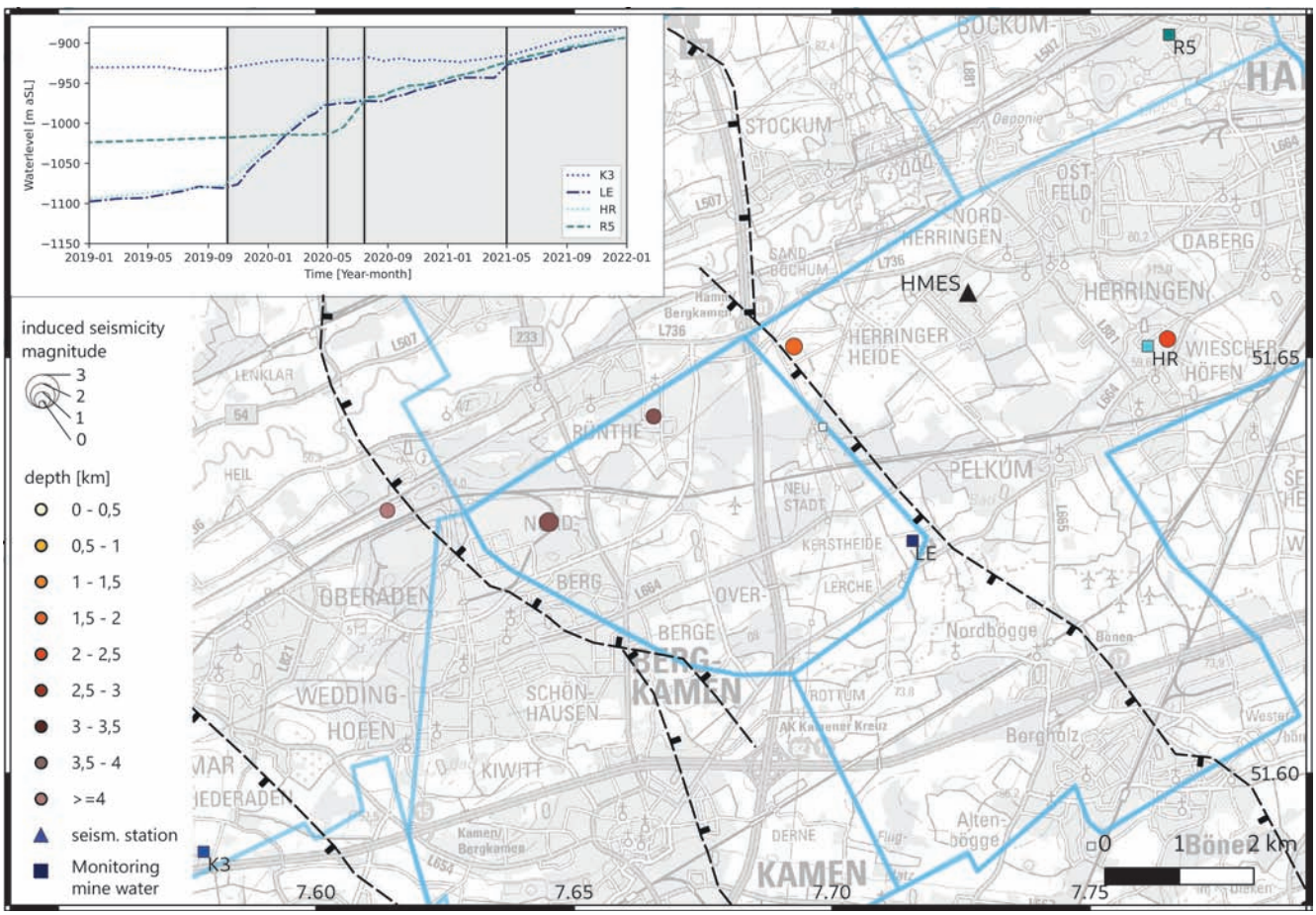

Fig. 7: Spatial distribution of induced earthquakes in phase 1 of the mine water rise (01/2019–09/2019): The curves in the inlet at the top left show the course of the water levels. The respective time period is highlighted in white. The graph of the water level at HR and LE increases slightly. On the map, only the seven strongest events are shown. Only these could be localised, since only one station was available in the epicentral area. Additionally, 40 smaller events without exact localisation were detected until the end of this phase.

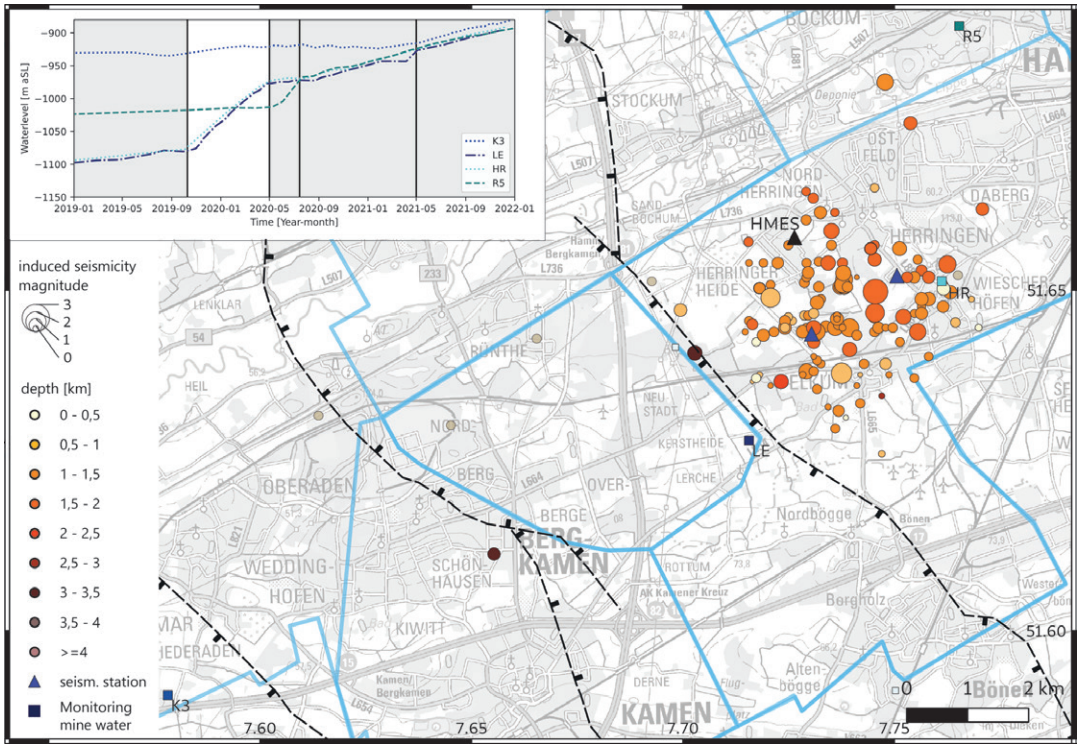

Fig. 8: Spatial distribution of induced earthquakes in phase 2 of the mine water rise (10/2019–04/2020): Strong parallel rise of levels at HR and LE from -1077 m to about -975 m in six months is observed. The two biggest events during flooding with M_{LV} 2.6 and 2.0 occurred in November 2019. The seismicity rate increases strongly, and events are located mainly in the area between LE and HR east of a major fault in Herringen and Pelkum.

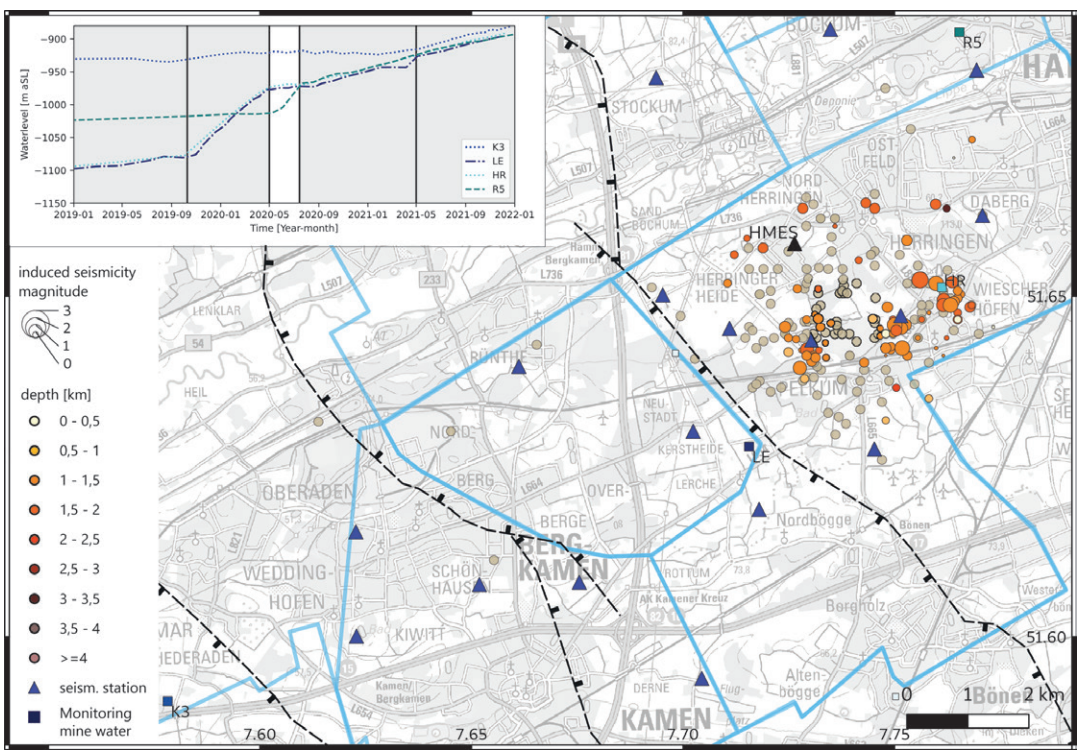

Fig. 9: Spatial distribution of induced earthquakes in phase 3 of the mine water rise (05/2020–07/2020): The previously rather constant level at R5 rises sharply and reaches the level of LE and HR, whose rise is slower again. The seismicity is localised in the same area as in the previous phase. Three spatial clusters emerge. There are few major events but a high number (2/3) of events M_{LV} <0.5.

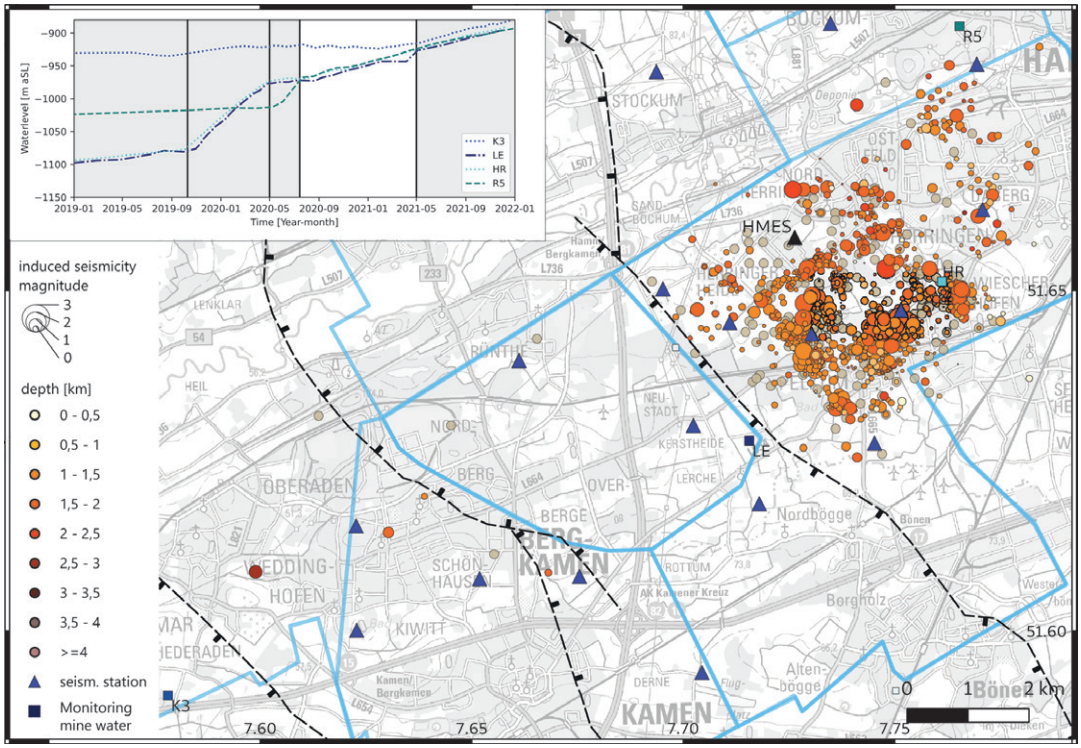

Fig. 10: Spatial distribution of induced earthquakes in phase 4 of the mine water rise (07/2020–04/2021): Moderate, simultaneous rise of levels at LE, HR and R5. Consistently high seismicity was observed. Most of the activity is localised in the same area as before, but an extension of the active area towards the north is visible.

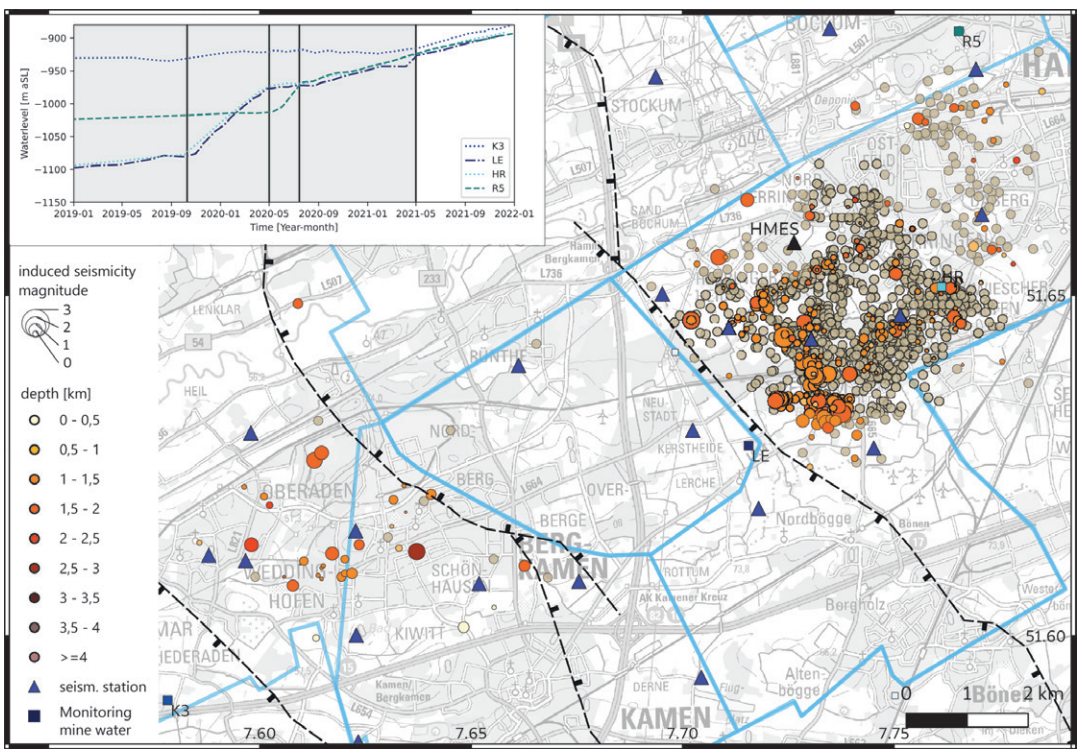

Fig. 11: Spatial distribution of the induced earthquakes in phase 5 of the mine water rise (05/2021–12/2021): Steady rise of the levels at the eastern monitoring stations LE, HR and R5. Beginning rise of the level at the monitoring station K3 in the central area of the dewatering. The seismicity in the active area between the eastern monitoring stations is mostly concentrated in several clusters in the area of the Flielicher Sprung at the western boundary of the main activity. Additionally, some quakes are observed in the area of Bergkamen in the central area of the dewatering. The area in between remains seismically inactive.

maps, the depths of the earthquakes are indicated by colours and their magnitude by the size of the dots. Events from the previous phases are shown in the background in uniform size and grey.

In phase 1 (01/2019–09/2019; Fig. 7), the level at HR and LE increases slightly. Only a few larger quakes with M_{LV} >0.9 can be seen on the map. Towards the end of this phase, another 40 smaller quakes were detected at the one station in the source region, but these could not be localised because no phases could be determined at the other available stations at a distance of at least 25 km. In the following 2nd phase (10/2019–04/2020; Fig. 8), a steep parallel increase of the levels at HR and LE (more than 100 m in 6 months) to about -975 m can be observed. During the same period, two induced events with M_{LV} 2.6 and 2.0 are measured in November 2019. The seismicity increases strongly and is mainly localised in the area between LE and HR, east of a larger fault in Herringen and Pelkum (districts of Hamm). The so far rather constant level at R5 rises strongly in phase 3 (05/2020–07/2020) and reaches the level of LE and HR, whose rise is slower again (Fig. 9). The seismicity is localised in the same area as in the previous phase. Three spatial clusters of seismicity emerge. There are few major events but a high number of events with M_{LV} <0.5. Fig. 10 displays phase 4 (07/2020–04/2021) where the increase of levels at LE, HR and R5 proceeds simultaneously at a moderate rate. Over this time period, the observed seismic activity is consistently high. Most of the seismicity is localised in the same area as before, but there is an extension of the active area northwards towards R5. During phase 5 (05/2021–12/2021) the increase of the levels at the eastern measuring stations LE, HR and R5 is constant (Fig. 11). An incipient rise of the level at the monitoring ring station K3 in the central area of the dewatering is detected. The seismicity in the active area between the eastern monitoring stations is mostly concentrated in several clusters at the western boundary of the main active region. In addition, some quakes are also observed in the Bergkamen area in the central area of the dewatering. The area in between is so far seismically inactive. There is no clear temporal trend in the depth of the events. The focal depths are concentrated in a range between 1,000 and 1,600 m (Fig. 12).

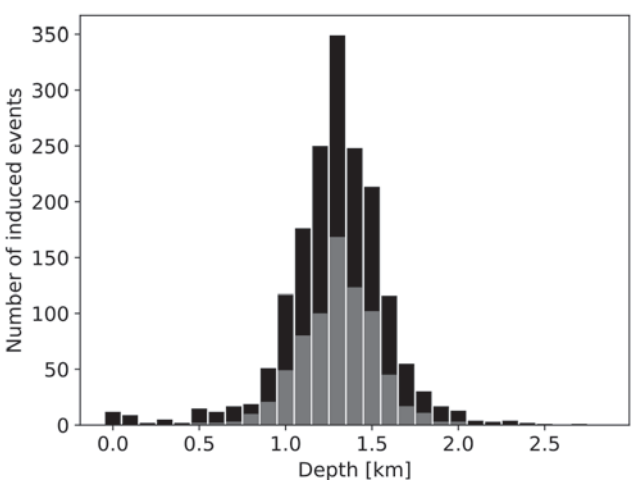

Fig. 12: Depth distribution of the evaluated seismicity in the study area in the period 6/2019–12/2021. The black bars show the total seismicity, the grey bars show only the events with a localisation uncertainty of less than 600 m in horizontal as well as vertical direction.

4. Geological setting and mining structures

The study area is divided into horst and graben structures by NNW–SSE striking normal faults. The main fault systems are the Königsborner Sprung in Bergkamen and the Fliericher Sprung between Bergkamen and Hamm. To the north and south, the region is bordered by WSW–ENE striking overthrusts (Geologischer Dienst NRW 2019). The faults show no recent tectonic activity.

The black shaded areas in Figs. 13 and 14 mark the longwall mining areas of the last ten years of mining from 2000 to 2010 (RAG-BID 2022). These are located in a depth range of 1,400–1,450 m in the Monopol mine and of 1,000–1,150 m in the Heinrich Robert mine (HR). The large differences in the depths of the mining sectors are due to the horst and graben structure of the area. Often the individual mining sections are separated by inclined rock headings (compare Fig. 2), which also represent barriers to the spreading of mine water. The bottom levels of each section of the combined mine (technical data of the RAG) are marked schematically in different shades of pink in the maps (Figs. 13, 14).

5. Discussion

A correlation between the increase in mine water and the reoccurring seismicity in the study area is clearly evident. A particularly high seismicity rate is observed when the mine water level has exceeded topographical barriers in the underground (Fig. 2) and the mine water no longer rises separately in the individual subareas. Questions on why the earthquakes occur, whether they correlate with known structures and if we can draw conclusions about the mechanisms arise.

In order to relate the seismicity to causes and structures, we only consider localisations whose horizontal and vertical localisation error is below 600 m. In Figs. 13 and 14, the earthquakes selected by the quality criterion are shown in full colour, with the entire catalogue transparent in the background. The geological fault systems and mining structures are also displayed in the figures.

Fig. 14 demonstrates particularly well that the seismicity is mainly confined to the area beneath and adjacent to the deep mining galleries (pink lines), which are already flooded. The shaded areas of the mining longwalls, in the immediate vicinity of which, above or below, the majority of the events were localised during active mining (Bischoff et al. 2010; Wehling-Benatelli et al. 2013) are largely devoid of seismicity. The fault zones also show no signs of seismic activity.

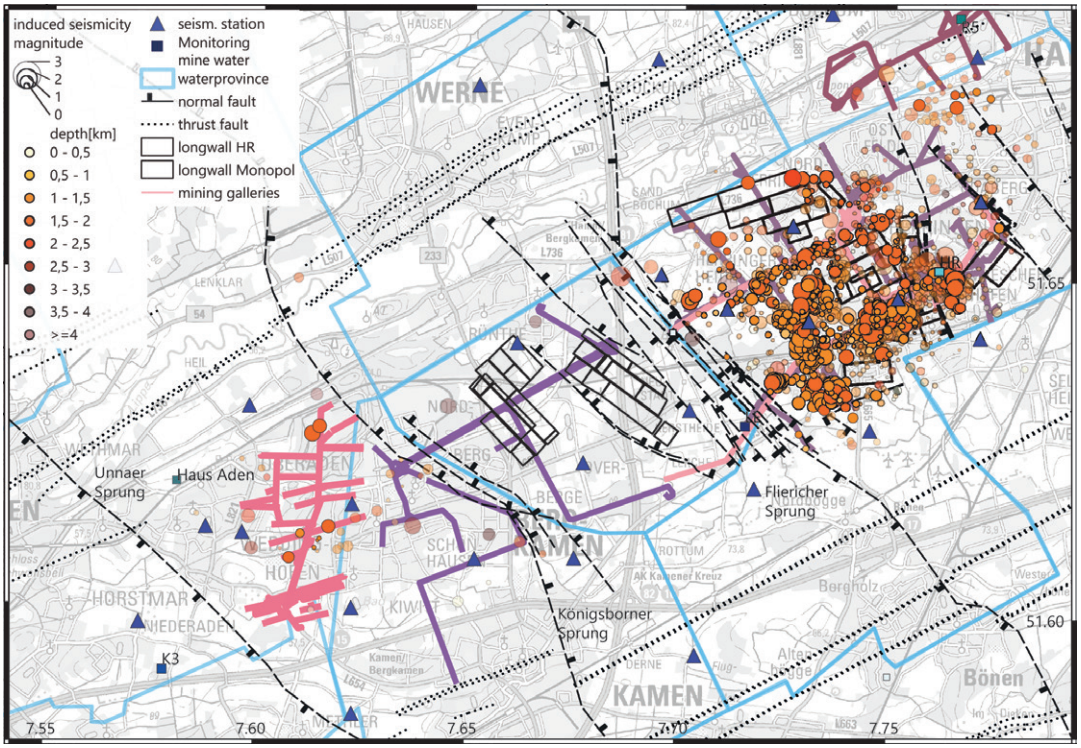

Fig. 13: This map of the study area shows both the measured seismicity from 06/2019–12/2021 and the system of relevant faults and mining structures. Mining galleries are marked in different shades of pink, representing the bottom levels of different mining sections or different depth levels in the range from 800 m to 1,120 m depth. The seismicity is shown here subdivided by quality criteria. Events with a localisation error below 600 m are depth-coded in solid colours. The events with a larger inaccuracy are shown semi-transparent in the background.

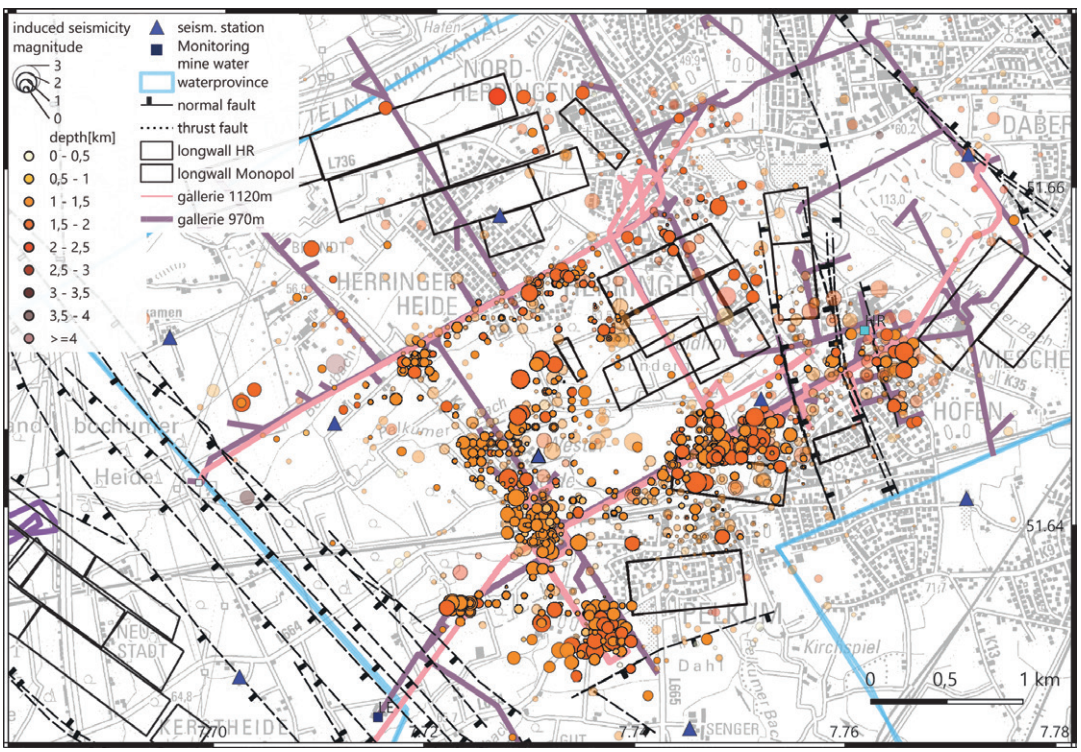

Fig. 14: The subarea around the former Heinrich Robert mine from Fig. 13 is shown here enlarged to visualise correlations between seismicity and structures in more detail. The clustering of seismicity in the area below the deep mining galleries is clearly visible.

Correlating the increase in mine water level with seismicity leads to the question, where the increase in pore fluid pressure due to mine water can alter the stress conditions in a way that seismic events are induced. Alber (2017) and Knoll (2016) describe two scenarios of failure that can lead to stress relief by seismicity during flooding. The first scenario is a failure caused by exceeding the rock strength and the second is the failure on zones of weakness by exceeding the shear strength, caused by the reduction of the effective normal stress by an increase of the pore fluid pressure. The first mechanism requires high water columns, while the second requires much lower pressures for activation. Alber (2017) concludes in his study that the second scenario, the reactivation of existing zones of failure is much more likely than the formation of new fractures.

During mining, according to Bischoff et al. (2010) and Wehling-Benatelli et al. (2013), most of the seismicity with small magnitudes (M_L <0.5) occurred near the active advancing face in the longwall, events of larger magnitude are associated with the failure of the sandstone benches mostly on the hanging wall above the active longwall and partly in the foot wall below the mine. In addition, a few events were associated by undermining and pillar failure. Some of these pre-damaged areas below the mine may now have been reactivated by the increase in pore fluid pressure. However, the seismicity clusters primarily below the bottom floors, which serve as the main waterways, rather than beneath or above the longwalls. Under the deepest flooded drifts, conditions appear to be particularly favourable for an increased pressure gradient. Because of the different locations, the failure mechanisms during flooding cannot be readily reconciled with those observed during mining.

The study by Alber (2017) predicts that the maximum magnitudes for flooding-induced seismicity in the Saar mining district are lower than the magnitudes of mining induced seismic events observed during the active mining phase when the same failure zones are reactivated. According to our seismicity distribution, which differs significantly in the mining phase and the flooding phase, such reactivation is not to be expected for most events in the eastern Ruhr area. The magnitudes in the flooding period, though, are also lower. The maximum magnitude determined for an event in the area of "Bergwerk Ost" colliery during mining is 3.0 M_L while the magnitude of the largest event observed at the beginning of the flooding is 2.6 M_L.

6. Conclusion

We combined data from the RUB's long-term seismic monitoring, the high-resolution FloodRisk monitoring network in the area of "Bergwerk Ost" colliery during flooding, and mine water measurements distributed in the study area. We were able to correlate the observed induced seismicity spatially and temporally with the rise in mine water and compared it with the seismicity during active mining.

Seismic activity was highest in the phase of active mining and concentrated in the vicinity of the mining areas. After the end of mining, only very low seismicity was detected. With the start of flooding, significantly more events were registered again. The number of events currently amounts to about a quarter of the seismicity detected during mining operations. Five different flooding phases were identified in which the correlated seismicity shows different distribution patterns. In these phases, a particular accumulation of events can be observed when the mine water level exceeds subsurface separations of waterways. Over the entire flooding period so far, the region below the deepest level in the area of the Heinrich Robert shaft in Herringen and Pelkum was most active. Generally, seismicity is predominantly localised below the flooded galleries of the bottom levels of the mine. Because of the different distribution of seismicity during active mining and during flooding, it can be concluded that the failure mechanisms are not identical. New mechanisms caused by a combination of the changed stress conditions due to mining in the dry regime and a now rising mine water have to be modelled and further investigated. The database of seismological events and mine water measurements presented here, which is still being expanded, provides a good basis to support such modelling with data.

7. Acknowledgements

The authors would like to thank all people and institutions that permit us to set up and operate our seismological stations on their premises. We would also like to thank the technicians of the RUB Observatory, Bernhard Klotz and Lothar Kühne, who helped setting up the stations and strive to keep them running trouble-free. We gratefully acknowledge the support of RAG and access to their digital service record and other data. We are especially appreciative of Ute Weissenborn for her role as contact person and for her assistance during the site visits to RAG. Many thanks to Janis Heuel, Marcel Paffrath and Anne Mohr for proofreading this work and their advice. We would like to thank the reviewers for their constructive criticism, suggestions for improvement and questions, which helped to further improve the manuscript.

This work was undertaken in the framework of the project FloodRisk (03G0893E) funded by the Federal Ministry of Educations and Research of Germany.

8. References

Alber, M. (2017). *Gutachten zur Erschütterungsentwicklung während des Grubenwasseranstiegs auf -320 m NN in den Wasserprovinzen Reden und Duhamel*. IHK Dortmund. Report. https://geodaten.rag.de/bid/tree/GenV/Saar/Wass_V/He_u_Ei_Grubw_DH/7_Alber_Ersch%C3%BCtterungen/Gutachten%20zur%20flutungsbedingten%20Ersch%C3%BCtterungenentwicklung%20Saar%20%2004_04_2017.pdf

Alber, M., Fritschen, R., Bischoff, M., & Meier, T. (2009). Rock mechanical investigations of seismic events in a deep longwall coal mine. *International Journal of Rock Mechanics and Min-*

ing Sciences, 46(2), 408–420. https://doi.org/10.1016/j.ijrmms.2008.07.014

Allgaier, F., Busch, B., Niederhuber, T., Quandt, D., Müller, B., & Hilgers, C. (2023). Fracture network characterization of the naturally fractured Upper Carboniferous sandstones combining outcrop and wellbore data, Ruhr Basin, Germany [this issue]. *Zeitschrift der Deutschen Gesellschaft für Geowissenschaften, 173*(4), 599–623. https://doi.org/10.1127/zdgg/2023/0369

Bischoff, M., Cete, A., Fritschen, R., & Meier, T. (2010). Coal mining induced seismicity in the Ruhr area, Germany. *Pure and Applied Geophysics, 167*(1-2), 63–75. https://doi.org/10.1007/s00024-009-0001-8

Cesca, S., Dahm, T., Juretzek, C., & Kühn, D. (2011). Rupture process of the 2001 May 7 M_W 4.3 Ekofisk induced earthquake. *Geophysical Journal International, 187*(1), 407–413. https://doi.org/10.1111/j.1365-246X.2011.05151.x

Cuenot, N., Dorbath, C., & Dorbath, L. (2008). Analysis of the microseismicity induced by fluid injections at the EGS site of Soultz-Sous-Forêts (Alsace, France): Implications for the characterisation of the geothermal reservoir properties. *Pure and Applied Geophysics, 165*(5), 797–828. https://doi.org/10.1007/s00024-008-0335-7

Dahm, T., Becker, D., Bischoff, M., Cesca, S., Dost, B., Fritschen, R., . . . Husen, S. (2013). Recommendation for the discrimination of human-related and natural seismicity. *Journal of Seismology, 17*(1), 197–202. https://doi.org/10.1007/s10950-012-9295-6

Foulger, G., Wilson, M., Gluyas, J., Julian, B., & Davies, R. (2018). Global review of human-induced earthquakes. *Earth-Science Reviews, 178*, 438–514. https://doi.org/10.1016/j.earscirev.2017.07.008

Friederich, W., Fischer, K. D., Rische, M., Hilgers, C., & Ruhr University Bochum (2020). *FloodRisk Seismic Network* [Data set]. Federal Institute for Geosciences and Natural Resources (BGR, Germany). https://doi.org/10.7914/SN/YD_2020

Fritschen, R. (2010). Mining-induced seismicity in the Saarland, Germany. *Pure and Applied Geophysics, 167*(1-2), 77–89. https://doi.org/10.1007/s00024-009-0002-7

Fritschen, R., Preuße, A., Brandt, K.-H., & Räkers, E. (1999). *Seismic events due to underground mining activities.* 18th International Conference on Ground Control in Mining, Lakeview Resort and Conference Center, Morgantown, WVa., USA.

Gal, M., Lotter, E., Olivier, G., Green, M., Meyer, S., Dales, P., & Reading, A. (2021). CCLoc – An improved interferometric seismic event location algorithm applied to induced seismicity. *Seismological Research Letters, 92*(6), 3492–3503. https://doi.org/10.1785/0220210068

Geologischer Dienst NRW (2019). *IS RK 10 KO: tectonic map of carboniferous faults, 10/2020, Data licence Germany – attribution – version 2.0*. https://www.opengeodata.nrw.de/produkte/geologie/geologie/RK/ISRK10

Greve, J., Busch, B., Quandt, D., Knaak, M., Hartkopf-Fröder, C., & Hilgers, C. (2023). Coupling heat conductivity and lithofacies of the coal-bearing Upper Carboniferous in the eastern Ruhr Basin, NW Germany [this issue]. *Zeitschrift der Deutschen Gesellschaft für Geowissenschaften, 173*(4), 673–695. https://doi.org/10.1127/zdgg/2023/0350

Harjes, H.-P. (1983–2004). *Registrierungen seismischer Ereignisse im Ruhrgebiet*. Institute of Geology, Mineralogy and Geophysics, Ruhr University Bochum.

Helmholtz Centre Potsdam GFZ, German Research Centre for Geosciences & gempa GmbH (2008). *The SeisComP seismological software package.* GFZ Data Services. https://doi.org/10.5880/GFZ.2.4.2020.003

Heuel, J., & Friederich, W. (2022). Suppression of wind turbine noise from seismological data using nonlinear thresholding and denoising autoencoder. *Journal of Seismology, 26*(5), 913–934. https://doi.org/10.1007/s10950-022-10097-6

Klose, C. D. (2012). Evidence for anthropogenic surface loading as trigger mechanism of the 2008 Wenchuan earthquake. *Environmental Earth Sciences, 66*(5), 1439–1447. https://doi.org/10.1007/s12665-011-1355-7

Knoll, P. (2016). Induzierte seismische Ereignisse beim Anstieg des Grubenwassers in stillgelegten Bergwerken – Geomechanische Charakteristika (16 pp.). *Leibnitz Online, 24*. https://leibnizsozietaet.de/wp-content/uploads/2016/09/Knoll.pdf

Lomax, A., Virieux, J., Volant, P., & Berge-Thierry, C. (2000). Probabilistic earthquake location in 3D and layered models. In C. H. Thurber & N. Rabinowitz (Eds.), Modern Approaches in Geophysics, 18: *Advances in seismic event location* (pp. 101–134). Dordrecht: Springer; https://doi.org/10.1007/978-94-015-9536-0_5

Lomax, A., Michelini, A., & Curtis, A. (2009). Earthquake location, direct, global-search methods. In R. Meyers (Ed.), *Encyclopedia of complexity and systems science* (pp. 2449–2473). New York: Springer; https://doi.org/10.1007/978-0-387-30440-3_150

Maibaum, F. (2012). *Wassertechnisches Feinkonzept zum Abschlussbetriebsplan der ZWH Ost.* Report.

Meier, T. (2005–2006). *Registrierungen seismischer Ereignisse im Ruhrgebiet*. Institute of Geology, Mineralogy and Geophysics, Ruhr University Bochum.

National Research Council. (2013). *Induced seismicity potential in energy technologies*. Washington, DC: National Academies Press; https://doi.org/10.17226/13355

Niederhuber, T., Kruszewski, M., Röckel, T., Rische, M., Alber, M., & Müller, B. (2023). Stress orientations from hydraulic fracturing tests in the Ruhr area in comparison to stress orientations from borehole observations and earthquake focal mechanism [this issue]. *Zeitschrift der Deutschen Gesellschaft für Geowissenschaften, 173*(4), 625–635. https://doi.org/10.1127/zdgg/2022/0352

Pechmann, J. C., Arabasz, W. J., Pankow, K. L., Burlacu, R., & McCarter, M. K. (2008). Seismological report on the 6 August 2007 Crandall Canyon Mine collapse in Utah. *Seismological Research Letters, 79*(5), 620–636. https://doi.org/10.1785/gssrl.79.5.620

Quandt, D., Busch, B., Fuchs, H., Alvarado de la Barrera, A., Greve, J., & Hilgers, C. (2023). Petrographical and petrophysical properties of tight siliciclastic rocks from the Ibbenbueren coal mine with regard to mine flooding [this issue]. *Zeitschrift der Deutschen Gesellschaft für Geowissenschaften, 173*(4), 653–672. https://doi.org/10.1127/zdgg/2022/0343

RAG AG (2014). *Konzept zur langfristigen Optimierung der Grubenwasserhaltung der RAG Aktiengesellschaft für Nordrhein-Westfalen, Herne* (29 pp.). https://www.bra.nrw.de/system/files/media/document/file/konzept_grubenwasserhaltung.pdf

RAG-BID (2022). *Ruhrkohle AG, Bürger Informations Dienst, Grubenwasser Monitoring*. https://geodaten.rag.de/mapapps/resources/apps/bid/index.html

Ruhr University (2007). *RuhrNet – Seismic network of the Ruhr University Bochum* [Data set]. Federal Institute for Geosciences and Natural Resources (BGR, Germany). https://www.fdsn.org/networks/detail/RN

Schütz, H., Mittag, R., Wallner, O., & Konietzky, H. (2014). *MAGS: Konzepte zur Begrenzung der mikroseismischen Aktivität bei der energetischen Nutzung geothermaler Systeme im tiefen Untergrund. Einzelprojekt 7: Prognose der möglichen induzierten/getriggerten Seismizität im Kristallin in Auswertung der flutungsbedingten seismischen Ereignisse im Bergbaurevier Aue/Schlema*. https://www.mags-projekt.de/MAGS/DE/MAGS1/Einzelprojekte/EP7/EP7_node.html

Seeber, L., Armbruster, J. G., Kim, W.-Y., Barstow, N., & Scharnberger, C. (1998). The 1994 Cacoosing Valley earthquakes near Reading, Pennsylvania: A shallow rupture triggered by quarry unloading. *Journal of Geophysical Research, 103*(B10), 24505–24521. https://doi.org/10.1029/98JB01497

Stammler, K., Bischoff, M., Brüstle, A., Ceranna, L., Donner, S., Fischer, K., . . . Wegler, U. (2021). German seismic and infrasound networks contributing to the European Integrated Data Archive (EIDA). *Seismological Research Letters, 92*(3), 1854–1875. https://doi.org/10.1785/0220200401

Talwani, P. (1997). On the nature of reservoir-induced seismicity. *Pure and Applied Geophysics, 150*(3-4), 473–492. https://doi.org/10.1007/s000240050089

Ukelis, O., Allgaier, F., Niederhuber, T., Rettenmaier, D., & Zorn, R. (2023). Kurzzeit-Bodengasmessungen zur Störungsdetektion – Schritt 1 für das nachbergbauliche Flutungsmonitoring [this issue]. *Zeitschrift der Deutschen Gesellschaft für Geowissenschaften, 173*(4), 637–651. https://doi.org/10.1127/zdgg/2022/0333

Wehling-Benatelli, S., Becker, D., Bischoff, M., Friederich, W., & Meier, T. (2013). Indications for different types of brittle failure due to active coal mining using waveform similarities of induced seismic events. *Solid Earth, 4*(2), 405–422. https://doi.org/10.5194/se-4-405-2013

Zoback, M. D., & Harjes, H.-P. (1997). Injection-induced earthquakes and crustal stress at 9 km depth at the KTB deep drilling site, Germany. *Journal of Geophysical Research, 102*(B8), 18477–18491. https://doi.org/10.1029/96JB02814

Manuscript received: 15.04.2022
Revisions required: 16.09.2022
Revised version received: 14.11.2022
Accepted for publication: 18.11.2022